Ball State Undergraduate Mathematics Exchange
`https://digitalresearch.bsu.edu/mathexchange`
Vol. 17, No. 1 (Fall 2023)
Pages 59 – 75

ICA can consistently bin similar sources together: The case with 3 sinusoidal sources separated into 2 components

Erin Munro Krull, Breanna Ollech, Kayley Grabowski*

Erin Munro Krull is an assistant professor in the department of mathematical sciences at Ripon College. Her research interests are in computational neuroscience, particularly data analysis and mathematical modeling applied to sleep and epilepsy.

Breanna Ollech worked on this paper as a senior at Ripon College studying Mathematics, Secondary Education and Exercise science. She is currently a first year mathematics teacher at OshKosh West High School. Along with teaching, she is also the softball coach and source of strength student mentor.

Kayley Grabowski worked on this paper as a senior at Ripon College studying Mathematics, Economics, and Business Management. She is currently a PhD candidate in Economics at the University of Illinois at Chicago. Outside of school, Kayley enjoys baking cookies, watching and playing sports, and being outdoors.

***Corresponding author:** munrokrulle@ripon.edu

Abstract

Independent Component Analysis (ICA) is a blind-source separation method, meaning that it takes in a recording with multiple sensors and attempts to unmix it into the original sources. For example, suppose there are 4 people (sources) speaking in a room with 4 microphones (sensors), then ICA unmixes the recording from the 4 microphones to give tracks of the individual people called ICA components. ICA is currently used to decompose a variety of signals with many sensors, including fMRI and EEG data. However, its use in interpreting data with fewer sensors, such as the local field potential (LFP), is limited because of concerns about how it handles over-complete data (data with more sources than sensors). While there has been some success in enhancing ICA so that it can extract more sources than sensors, we focus on how ICA handles over-complete data. In this paper, we show that ICA consistently bins sources with similar spatial maps together when there are 3 sinusoidal sources and 2 sensors.

1 Introduction

Many neurophysiological recordings of the brain used to study micro-circuits include the local field potential (LFP). There are a wide variety of LFP recordings freely available [45], as well as recent technological developments in recording the LFP [19, 22]. One of the benefits of field potential recordings is that they often simultaneously record nearby action potentials along with field potentials reflecting the summation of many cells acting at once, some possibly from far away [26, 46]. While these recordings may have limited spatial resolution, they tend to have very high time resolution. Standard methods of decomposing the LFP for further analysis include spectral analysis, which addresses frequency content, and current source density, which uses field potential physical properties to derive current sources and sinks. Another decomposition method is independent component analysis (ICA), which can be used to separate overlapping sources that contributed to the recording. For example, suppose there are two voices recorded over two microphones, so that their amplitude differs on each microphone. By taking advantage of the distinct voices and their spatial differences in amplitude, ICA attempts to separate the two-sensor recording so that each component contains an individual voice. (See figure 1 for an illustration.)

ICA is one of many methods of blind-source separation. While there are many resources describing this method in detail [6, 24, 25], we will briefly describe the framework here using the LFP as an example. Suppose there are n sources $\vec{s}(t) = \begin{bmatrix} s_0(t) & s_1(t) & \dots & s_{n-1}(t) \end{bmatrix}$ affecting the LFP, and the LFP is recorded by an electrode with n sensors $\vec{x}(t) = \begin{bmatrix} x_0(t) & x_1(t) & \dots & x_{n-1}(t) \end{bmatrix}$. ICA will take the data from the sensors, and separate them into n components $\vec{c}(t) = \begin{bmatrix} c_0(t) & c_1(t) & \dots & c_{n-1}(t) \end{bmatrix}$ so that the time series of the components are as statistically independent as possible. ICA assumes that sources are mixed linearly onto each sensor. That means ICA assumes there is some mixing matrix M so that $\vec{x} = M\vec{s}$, where the columns of M represent the source spatial maps or relative amplitude across sensors. Likewise, ICA decomposes signals by returning an unmixing matrix U, so that $\vec{c} = U\vec{x}$. Assuming all the original sources are independent, then $\vec{c}(t)$ is a linear estimate of $\vec{s}(t)$. Unlike the other common decomposition methods principal component analysis (PCA) or factor analysis (FA), ICA does not necessarily make restrictions on whether the spatial maps of the components are oriented at right-angles, and doesn't necessarily favor high-amplitude directions. This makes ICA a relatively flexible decomposition method, which is used in many fields besides neuroscience [36], including analytical chemistry [33], cancer omics datasets [43], gravity and magnetic signal processing [49], and image processing [4, 9, 10].

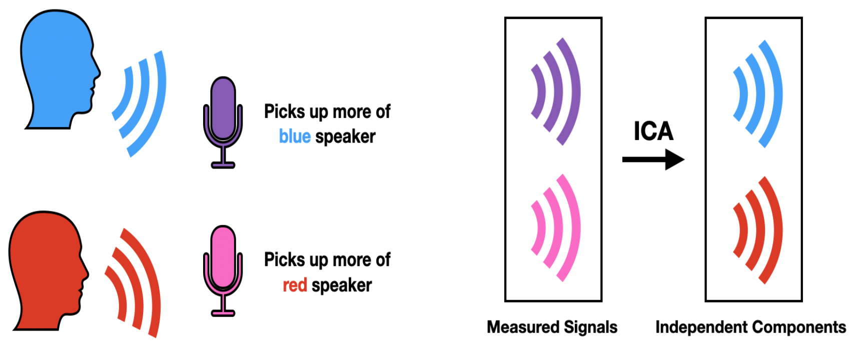

Figure 1: Illustration of ICA A) Different sources have differing amplitudes on each sensor. Therefore, each sensor will have its own mixture of all sources. In this illustration, the top microphone picks up more of the blue speaker than the red speaker, so its voice mixture is represented as deep purple. At the same time, the bottom microphone picks up more of the red speaker than the blue speaker, so its mixture is represented as fuchsia. B) ICA attempts to separate sources so they are as independent as possible. In this case, ICA would take the recorded mixtures and attempt to separate them into components containing the original voices. (Figure originally published in [44], reprinted with permission.)

ICA is relatively straightforward to interpret if the recording involves a lot of sensors. If there are more sensors than sources, then higher amplitude components may summarize major sources (above the signal-to-noise ratio), while smaller amplitude components may represent noise in the recording. Currently, ICA is used to analyze a variety of neurophysiological data, including fMRI [8], MRI [50], MEG [5], EEG [3, 36], voltage sensitive dye [1, 14, 21, 39], and PET [48]. Many of these data sets have an abundant number of sensors that are assumed to be greater than the number of relevant sources, and there is research on how to choose a subset of ICA components so that they are reliable and match biologically plausible or known sources [11, 13, 31, 51]. There are several studies that use ICA to interpret LFP data, even though these recordings tend to have fewer sensors [20]. However, these studies cannot necessarily assume that there are fewer relevant sources than sensors.

While ICA is thought to work well if there are no more sources than sensors, it is still unclear how ICA handles over-complete or under-determined data where there are more sources than sensors. Several methods try to address this issue by modifying the ICA algorithm so that more sources are extracted, possibly taking advantage of sparseness or other features in the data [36]. There are other studies which demonstrate that ICA can produce consistent results, across multiple ICA runs and subjects, even when data is over-complete [2, 13, 15, 25, 27, 28, 32, 35]. While some of these studies compare ICA components by measuring similarity between spatial maps, none of these address how and why certain sources may be combined into a single component. The uncertainty in how to interpret ICA components extracted from over-complete data, along with some instability of ICA components, may be the reason why ICA is not always recommended as an analysis tool for decomposing LFP. Reviews may instead point to decompositions which rely more on spectral analysis or on forward models of known biophysical structures [12, 17, 19, 29, 38, 41, 47]. On the other hand, ICA is more readily used in studies involving EEG [2, 3, 30] and fMRI [48, 42], where recordings tend to contain many more sensors.

We focus on describing how ICA handles over-complete data. In particular, we ran simulations to test how ICA separates 3 noisy sinusoidal sources recorded on 2 sensors into 2 components. Our results show that ICA can separate sources in a predictable manner, namely sources with similar spatial maps across the sensors are binned together. There is very little variation in how sources are binned together across different ICA runs, as long as 2 of the 3 sources are closer together in terms of their spatial map. If all 3 sources have equidistant spatial maps, then we see more variation between ICA runs. Our results indicate we may be able to determine how ICA bins original sources together by looking at the reliability and spatial maps of ICA components over the sensors. Moreover, viewing ICA components as binned sources may have advantages in interpreting the original data. For example, in a recording of a 4-part chorus, we may be more interested in components that contain the 4 voice parts, not the individual voices.

2 Methods

We ran simulations using Google Colaboratory[1], which used Python version 3.6.9. For each simulation, we used the same 3 sources:

$$\begin{aligned} s_0 &= \sin(2\cdot 2\pi t) + \text{random noise} \\ s_1 &= \sin(3\cdot 2\pi t) + \text{random noise} \\ s_2 &= \sin(5\cdot 2\pi t) + \text{random noise} \end{aligned}$$

where the random noise is uniformly distributed over $[-0.5, 0.5]$. Our 3 sources are illustrated in figure 2. We used sinusoidal functions with relatively prime frequencies so we could easily distinguish which sources were separated into which components using Fourier analysis. We added non-Gaussian noise at the same amplitude as the sinusoidal function to help satisfy the conditions of ICA, which are that original sources are independent and non-Gaussian. Without noise, we may see a pattern in the data since the combined signals repeat every $2\cdot 3\cdot 5$ seconds. With the added noise, we will see that these signals appear fairly independent when plotted against each other. For our analysis, all sources were sampled at 1000 Hz, and recorded for 100 s.

We mixed the sources onto two sensors using a mixing matrix M of the following

[1] Google Research, `https://colab.research.google.com`, accessed June 2022

form:

$$M = \begin{bmatrix} \vec{m}_0 & \vec{m}_1 & \vec{m}_2 \end{bmatrix} = \begin{bmatrix} \cos(\alpha_0) & \cos(\alpha_1) & \cos(\theta) \\ \sin(\alpha_0) & \sin(\alpha_1) & \sin(\theta) \end{bmatrix}$$

so that the recorded data mixtures are $\vec{x}(t) = M\vec{s}(t)$. The angles α_0, α_1, and θ in our mixing vectors represent the spatial map or relative amplitude of the original sources on each sensor. For instance, an angle of $0°$ means the source is recorded entirely on the first sensor, while an angle of $90°$ means the source is recorded entirely on the second sensor. All other angles represent how the source is distributed across both sensors. Angles that are $> 90°$ or $< -0°$ represent mixtures where the source sign is flipped from one sensor to another, which can frequently occur in voltage recordings.

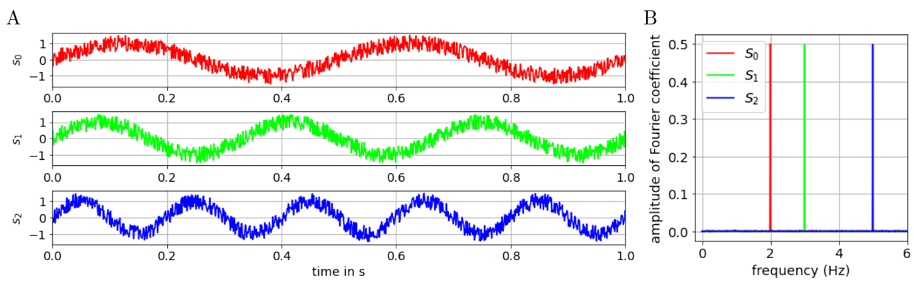

Figure 2: Figure 2: Original sources A) Time series of the 3 original sources. Each source is a sine wave at a different frequency combined with uniform noise. We used the same sources in all simulations. B) The amplitude of the Fourier transform of each source.

While the mixing vectors in M all have an amplitude of 1, the same data mixture can be produced by any reciprocal pair of mixing vectors and sources. For example, the negative mixing vector and matching source would produce the same mixture:

$$\begin{bmatrix} -\vec{m}_0 & \vec{m}_1 & \vec{m}_2 \end{bmatrix} \begin{bmatrix} -s_0 \\ s_1 \\ s_2 \end{bmatrix} = -\vec{m}_0(-s_0) + \vec{m}_1(s_1) + \vec{m}_2(s_2) = \vec{x}$$

Similarly, if we scale one mixing vector by a constant k and its source by $1/k$, we would also get the same data mixture. For this reason, the scaled mixing vector $k\vec{m}_i$ is considered equivalent to the unit vector $\vec{m}_i$ and we can use the angle to represent the spatial map for both vectors. Moreover, since $-\vec{m}_i$ is equivalent to $\vec{m}_i$, then we only consider angles from $-45°$ to $135°$.

We ran several cases, where we focus on a fixed α_0 and α_1 and vary θ from $-45°$ to $135°$. For each value of θ, we apply ICA to the data mixture 10 times, using both the FastICA algorithm [37] and the extended infomax algorithm ([16], Version 1.2.1: 10.5281/zenodo.7314185). The algorithm returns the un-mixing matrix U and estimated mixing matrix $M_{\text{est}} = U^{-1}$. Note that M_{est} is both the mixing matrix of the ICA components and the algorithm's best attempt at estimating M with a 2×2 matrix. We calculated the angles of the estimated mixing vectors within M_{est}, and compared them to the angles of the original mixing vectors.

We also applied the discrete Fourier transform to the ICA components [18], and compared the frequency content of the components with the original sources by calculating the relative amplitude as follows: Let $|y_i(t)|$ be the root mean square (RMS) amplitude of a signal $y_i(t)$, and $Y_i(\omega)$ be the Discrete Fourier transform coefficient of the signal at frequency ω Hz. Then the relative amplitude for frequency ω in component $c_i(t)$ compared to the original source $s_j(t)$ is $\frac{|C_i(\omega)|/|c_i(t)|}{|S_j(\omega)|/|s_j(t)|}$.

3 Results

3.1 A detailed case: spatial maps of the first two sources are 90° apart.

For our first case, we show what happens in detail with 2 sources and 2 sensors when $\alpha_0 = 0^\circ$ and $\alpha_1 = 90^\circ$, and with 3 sources and 2 sensors where $\theta = -30^\circ$ for the third source. We used the FastICA algorithm for all results shown below. The extended infomax algorithm yielded nearly identical results. Figure 3 shows the data mixtures presented to ICA, along with the time series for the components $U\vec{x}(t) = \vec{c}(t)$ and their Fourier transforms. Note that, while we give the ICA algorithm the entire data mixture, ICA disregards all time information. For example, in the 2-source case, the algorithm only takes the data set shown in figure 3Ai into account. ICA appears to separate the 2 sources mixed onto 2 sensors perfectly. On the other hand, the 2-dimensional data mixture of the 3 sources appears to be separated so that source s_1 is contained in c_0 while sources s_0 and s_2 are mostly contained in c_1. It appears that s_1 is separated out of c_1 entirely, while c_0 contains some amount of the frequencies found in s_0 and s_2, though not enough to cloud s_1.

To compare the ICA components with the original sources further, we also looked at the estimated mixing matrix $M_{\text{est}} = U^{-1}$, whose columns are mixing vectors which represent the ICA component's spatial map or relative amplitude across the sensors. Both the original mixing vectors and the estimated mixing vectors are shown in figure 4. Since the scale of the mixing vectors doesn't affect the spatial maps, as explained in Methods, we can represent them with an angle between -45° and 135°.

We combine the frequency and angle comparisons, as shown in figure 5. The angles illustrate how the spatial map of the original sources may be binned in the ICA components. Frequency content is represented by color, where the relative amplitude of each frequency is represented by color intensity. With these comparisons, we see that the separation for 2 sources is very close to the original sources. Likewise, for 3 sources one ICA component is almost entirely dedicated to the original source with angle 90°, while the other two sources are binned in terms of both angle and frequency content. In fact, figure 5 shows results for 10 ICA runs, overlaid on top of each other. These results show that there is very little variation between ICA runs for these data mixtures.

We now expand our analysis so that θ varies from -45° to 135°. Figure 6 shows three cases where α_0 and α_1 are 90° apart. We see in all of these cases that the ICA components follow the original sources in both angle and frequency content. The ICA components tend to bin together whichever sources have spatial maps with closer

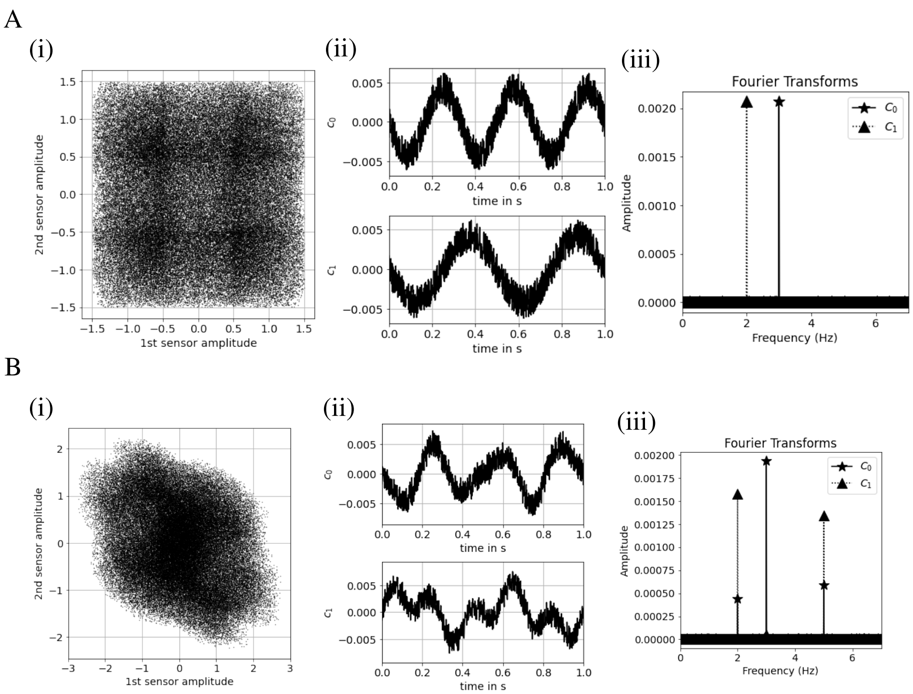

Figure 3: ICA applied to mixtures with 2 or 3 sources A) (i) The data mixture with 2 sources, $\alpha_0 = 0°$, and $\alpha_1 = 90°$. This is the same data where s_0 is recorded entirely on the first sensor and s_1 is recorded entirely on the second sensor. (ii) Example ICA components. Components can be returned in either order, and may be scaled differently than the original sources. Both of these components are negative relative to the original sources. (iii) The amplitude of the component Fourier coefficients confirm that the sources are separated very well, with each component almost entirely containing a single frequency. B) (i) The sources s_0, s_1, and s_2 mixed onto the two sensors using M with $\alpha_1 = 0°$, $\alpha_2 = 90°$, and $\theta = -30°$. (ii) Example ICA components. The first component c_0 appears to contain mostly s_1 (which oscillates at 3 Hz), while the second component c_1 appears to be a mixture of s_0 and s_2. (iii) The amplitude of the component Fourier coefficients confirm that c_0 is predominantly composed of s_1, but also contains some of the other sources. We also see that c_1 contains a fairly even amount of s_0 and s_2 since their frequency amplitude is about the same.

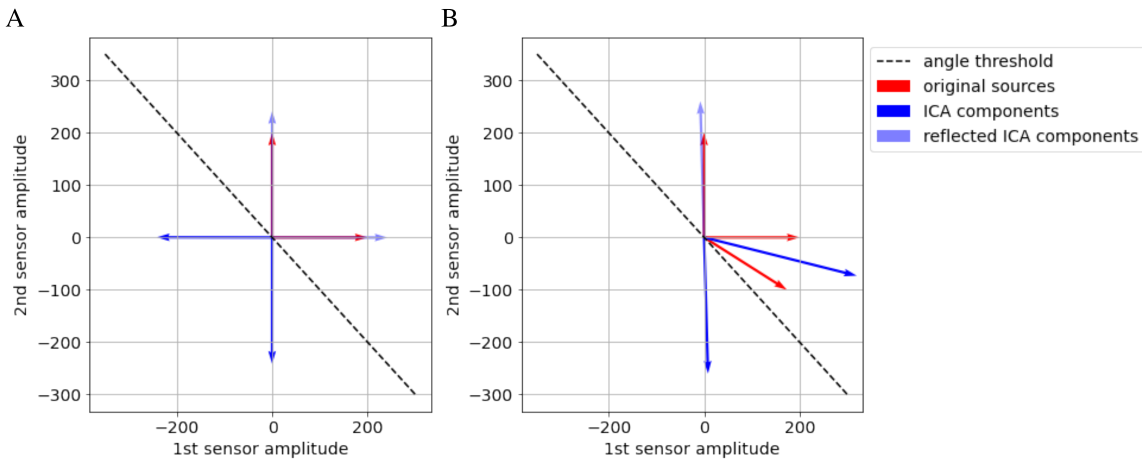

Figure 4: Angles represent the spatial map or relative amplitude over sensors. A) Mixing vectors representing the spatial maps of sources s_0 and s_1 on each sensor (red, magnified 200 times), along with vectors representing the spatial maps of ICA components as reported in M_{est} (shown in blue). We use these vectors to calculate the angles for the original sources and the ICA components. In our analysis, if the component amplitude vector has angle $< -45°$ or $> 135°$ then we reflect the vector across the origin. B) Mixing vectors representing the spatial maps of the original 3 sources on each sensor (red, magnified 200 times), along with the ICA components (blue). From these vectors, it appears that ICA separated s_1 into a single component, and s_0 and s_2 into the other component, similar to figure 3.

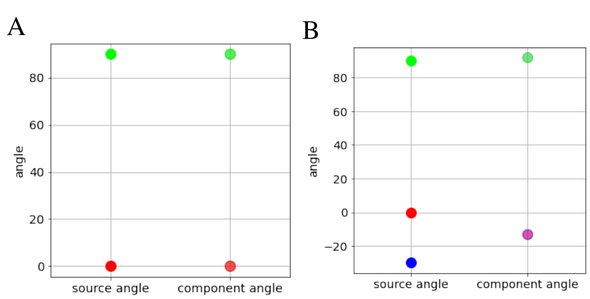

Figure 5: Comparison of angle and frequency distribution for $\alpha_1 = 0$, $\alpha_2 = 90$, $\theta = -30$ degrees. Angles for the spatial maps of the original sources are on the left, while angles for the ICA component spatial maps are on the right. Color indicates the relative amplitude of different frequencies: red for 2 Hz, green for 3 Hz, and blue for 5 Hz. Both panels show trials for 10 ICA decompositions, where the marker for each run has opacity set to 1/10. A) Two sources and two sensors. B) Three sources and two sensors.

angles. Since -45° is considered equivalent to 135°, then angles may be closer across this angle threshold. There appears to be almost no variation between ICA runs. The only instance with some variation is where θ is half-way between α_0 and α_1.

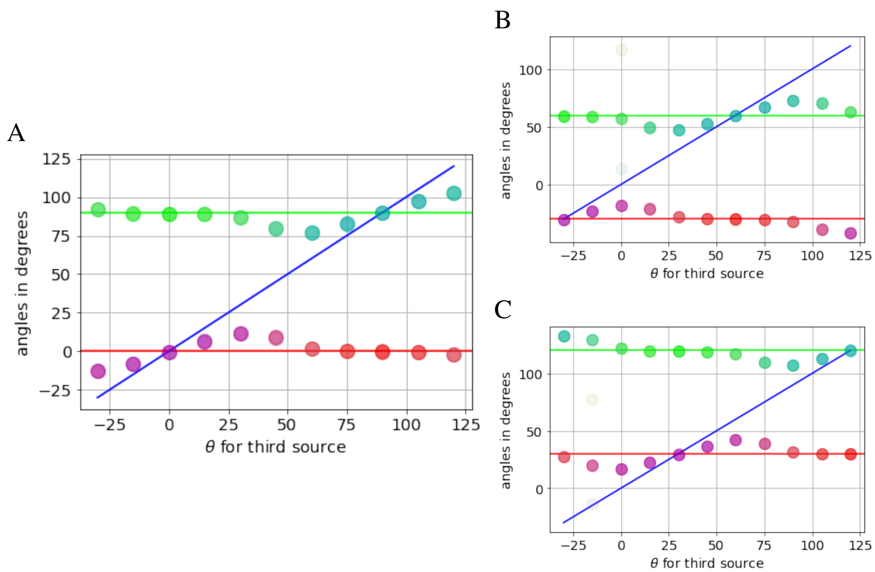

Figure 6: Comparison of angle and frequency distribution: base angles are 90° **apart.** Solid lines represent the spatial map angle of the original sources, along with their color-coded frequency: red for 2 Hz, green for 3 Hz, and blue for 5 Hz. Dots represent the angle and frequency content for the ICA components, similar to figure 5. A) Results for ICA runs with θ ranging from -30° to 135° when $\alpha_0 = 0$ and $\alpha_1 = 90^\circ$. B) Results for $\alpha_0 = -30^\circ$ and $\alpha_1 = 60^\circ$. C) Results for $\alpha_0 = 30^\circ$ and $\alpha_1 = 120^\circ$.

3.2 Cases where spatial maps of the first two sources are less than 90° apart.

Figure 7 shows results for cases where α_0 and α_1 are 60° apart. The ICA components still follow the original sources in most cases. However, now that α_0 and α_1 are 60° apart, it is possible for all three angles to be equidistant over the 180° range. When they are equidistant, we see a lot more variability between ICA runs using the FastICA algorithm. This makes sense since there is no true optimal separation of sources if they are equidistant. The results for the extended infomax algorithm didn't show as much variety, but instead showed some discontinuity in results when the sources are equidistant. (See figure 1.1 in the appendix.) There may be more variability in the results for values of θ in between the ones chosen.

Figures 8 and 9 show results where α_0 and α_1 are 45° apart and 30° apart, respectively. When α_0 and α_1 are 45° apart, we still see some variability between ICA runs when the angles are more equidistant, but the majority of the ICA runs return components that bin together the original sources with the closest angle. When α_0 and α_1 are 30° apart, we see almost no variability, similar to the case where α_0 and α_1 are 90° apart.

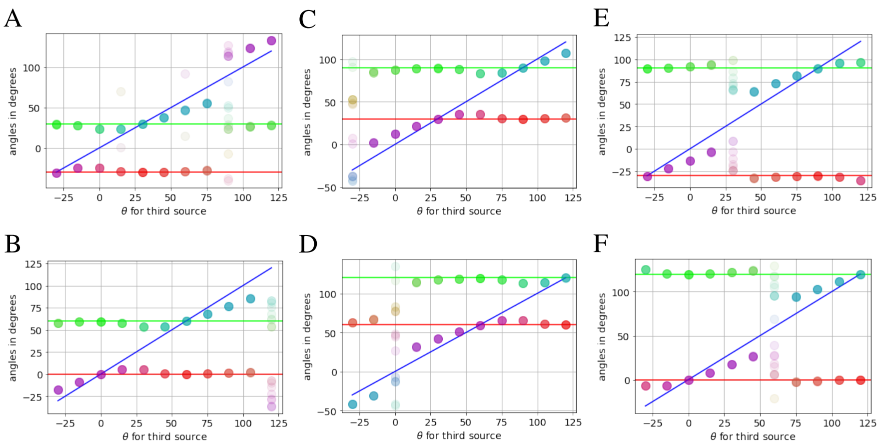

Figure 7: Comparison of angle and frequency distribution: base angles are 60° **apart.** Results where all combinations of α_0 and α_1 are 60° apart, starting with $\alpha_0 = -30^\circ$ and $\alpha_1 = 30^\circ$. Since angles that are 180 degrees apart are equivalent, then we also consider cases where the angle is 60° apart across the boundary: $-45^\circ = 135^\circ$. For instance $\alpha_0 = -30^\circ = 150^\circ$ and $\alpha_1 = 90^\circ$ are also 60° apart. Since all possible angles span 180°, we see the greatest instability when the 3 sources are all equidistant at 60°.

In line with previous examples where ICA bins sources with the closest angle together, the original sources with spatial map angles α_0 and α_1 are binned together until θ is within 30° of either angle.

4 Discussion

We applied the ICA algorithm to 2-sensor data mixtures composed of 3 noisy sinusoidal sources. The spatial map of each source across the sensors is characterized by the angle of its mixing vector. We found that ICA systematically binned sources with the closest angle together. ICA would evenly split sources if one source's angle was equidistant to the other two. The ICA components were stable across multiple ICA runs in most cases. The largest variability was seen when all 3 source angles were equidistant. Our results give evidence that ICA predictably separates sources and that ICA components can be interpreted as estimated *groups* of original sources.

While we examined the stability of ICA components systematically based on their spatial maps, several other studies demonstrated the stability of ICA components with biologically plausible data [2, 25, 13, 15, 27, 28, 32]. Also, while we examined how ICA components bin sources together by their spatial maps, there are several methods that compare ICA spatial maps to choose the ideal number of components when there are an abundant number of sensors [11, 23].

Understanding how ICA bins sources together may shed light on how best to use ICA to decompose data. Researchers can run ICA multiple times to see whether ICA

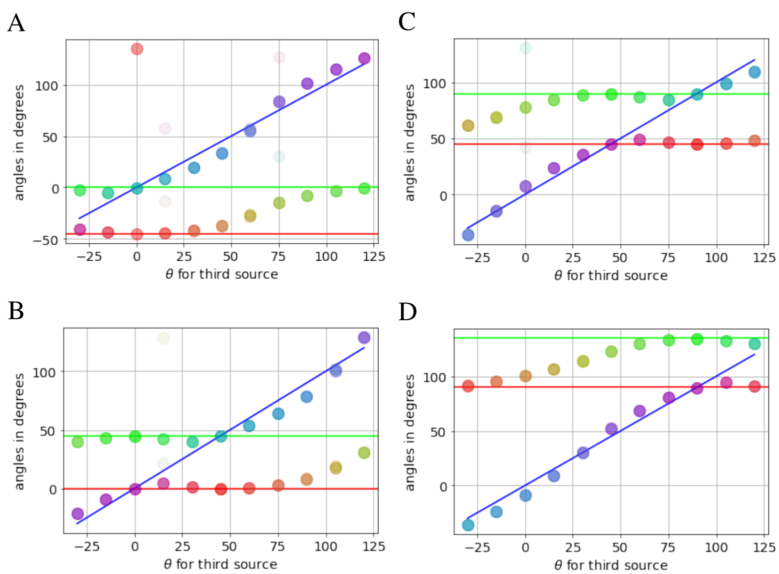

Figure 8: Comparison of angle and frequency distribution: base angles are 45° **apart.** We see more stability when the base angles are closer together. However, there are some cases with instability when all 3 sources are close to equidistant.

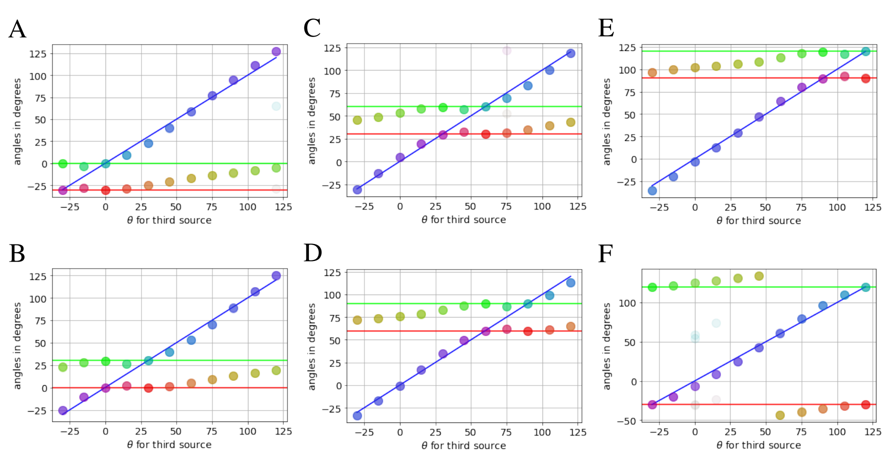

Figure 9: Comparison of angle and frequency distribution: base angles are 30° **apart.** Source separation appears very stable when two sources are significantly closer together.

components are consistent across ICA runs [32]. If the ICA components have a high degree of variability, then the underlying original sources may have equidistant spatial maps. While we defined distance using the dot product, other studies have used a variety of different measures to compare spatial maps [11, 27]. If there are equidistant sources, decreasing the total number of components may bin the equidistant sources together so that the ICA components are more stable. ICA components may also be more stable by increasing the total number of components enough to resolve equidistant sources. If there are fewer sensors than desired ICA components, this may be done with a reliable method to extract more sources than sensors.

The idea that ICA bins sources together can help address the consistency of ICA components across different recordings. For instance, suppose we have a set of 10 LFP recordings, each taken from a different animal under the same context, so we have the same number of neurophysiological sources. Suppose further that each recording used 32 sensors, but that some of the sensors are faulty in 5 of the recordings. The faulty sensors still pick up the LFP, but their baseline voltage drifts - which can happen often since neural electrodes are highly sensitive. These faulty sensors add an extra source, which ICA may pick out as a single component since the spatial map is concentrated on one sensor - making it very distinct from other spatial maps. This leaves fewer components for the neurophysiological sources. So some of the neurophysiological sources that ICA separated in recordings without faulty sensors may be binned together in recordings with faulty sensors. We may be able to tell which sources are binned together by looking at their spatial maps. Most current studies that use ICA on LFP focus on large-amplitude, easily replicable components. Unlocking which components are binned together may allow a better interpretation of smaller-amplitude components.

Seeing how ICA bins sources together can help ICA components be seen as relevant functional groups of sources. These functional groups may not necessarily be neuronal populations, but may represent afferent synapses, active cell parts such as dendrites, glia, or cell assemblies [7, 34, 35, 40, 41]. We may even be able to quantify how well sources are separated from each other based on the relative distance between the spatial maps of the ICA components.

Our results represent an initial study in how ICA treats over-complete data, where we focus on 3 sinusoidal sources with the same amplitude separated into 2 components. We used the same 3 sources for all of our simulations. Future work in this area could consider many different types of sources that vary in frequency spectrum and amplitude, along with different combinations in the number of sources and components. In particular, natural sources can include a whole range of frequencies at varying amplitudes. If two sources share some of the same frequencies, then ICA may have a harder time distinguishing between the two sources. Also, ICA normalizes the data given to it so that amplitudes in all directions are the same. This means lower-amplitude sources may not be normalized if they are not mixed in a distinct direction. Therefore, ICA may bin sources differently in over-complete data if some of the sources have much higher amplitude than others. We used the FastICA algorithm and the extended infomax algorithm in all our simulations. While the results using both of these algorithms were nearly identical, we did note some differences in ICA component stability when spatial maps are equidistant. Other ICA algorithms may yield different results in the amount of variability between ICA runs as well as distribution of angles between components.

ICA is designed to separate sources so that components are as independent as possible. The idea that ICA bins similar sources together not only follows this goal, but can allow for more insightful interpretation of separated sources. Indeed, binning sources together may be the most desirable outcome. For example, in the LFP we may be more interested in separating functional groups of neurons than many individual neurons with similar activity. While current studies that use ICA in interpreting the LFP tend to focus on just a few replicable components, ICA separation allowed them to have insights that may not have been possible by other means. Therefore, using ICA may allow immediate insights into micro-circuits in the brain.

1 Results for the extended infomax algorithm when base angles are $60°$ apart.

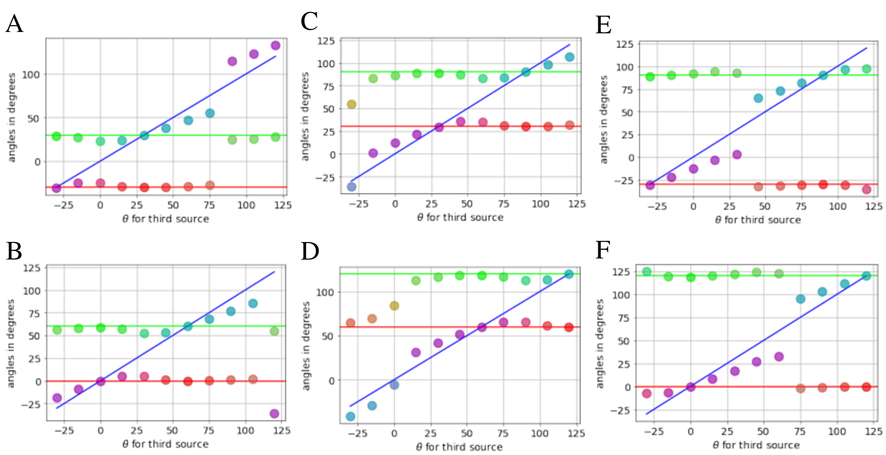

Figure 1.1: Comparison of angle and frequency distribution using the extended infomax algorithm: base angles are $60°$ apart. Instead of the instability we see with the FastICA algorithm, results tend to jump discontinuously. However, we may see some instability if we try finer-grained values for θ.

Bibliography

[1] Aimon, S., Katsuki, T., Jia, T., Grosenick, L., Broxton, M., Deisseroth, K., Sejnowski, T. J., and Greenspan, R. J. (2019). Fast near-whole–brain imaging in adult Drosophila during responses to stimuli and behavior. *PLoS Biology,* 17(2):e2006732.

[2] Artoni, F., Menicucci, D., Delorme, A., Makeig, S., and Micera, S. (2014). RELICA: A method for estimating the reliability of independent components. *NeuroImage,* 103:391–400.

[3] Babiloni, C., Barry, R. J., Başar, E., Blinowska, K. J., Cichocki, A., Drinkenburg, W. H., Klimesch, W., Knight, R. T., Silva, F. L. d., Nunez, P., Oostenveld, R., Jeong, J., Pascual-Marqui, R., Valdes-Sosa, P., and Hallett, M. (2019). International Federation of Clinical Neurophysiology (IFCN)– EEG research workgroup: Recommendations on frequency and topographic analysis of resting state EEG rhythms. Part1: Applications in clinical research studies. *Clinical Neurophysiology,* 131(1):285–307.

[4] Bartlett, M. S., Movellan, J. R., and Sejnowski, T. J. (2002). Face Recognition by Independent Component Analysis. *IEEE Transactions on Neural Networks*, 13(6):1450.

[5] Bénar, C.-G., Velmurugan, J., López-Madrona, V., Pizzo, F., and Badier, J. (2021). Detection and localization of deep sources in magnetoencephalography: a review. *Current Opinion in Biomedical Engineering*, 18:100285.

[6] Brown, G. D., Yamada, S., and Sejnowski, T. J. (2001). Independent component analysis at the neural cocktail party. *Trends in Neurosciences,* 24(1):54–63.

[7] Buzsáki, G., Anastassiou, C. A., and Koch, C. (2012). The origin of extra cellular fields and currents-EEG, ECoG, LFP and spikes. *Nature Reviews Neuroscience,* 13(6):407–420.

[8] Calhoun, V. D. and Lacy, N.d. (2017). Ten Key Observations on the Analysis of Resting-state Functional MR Imaging Data Using Independent Component Analysis. *Neuroimaging Clinics of North America,* 27(4):561–579.

[9] Calinon, S. and Billard, A. (2005). Recognition and reproduction of gestures using a probabilistic framework combining PCA, ICA and HMM. In *Proceedings of the 22nd International Conference on Machine Learning*, ICML'05, page105–112, NewYork, NY, USA. Association for Computing Machinery.

[10] Cvejic, N., Bull, D., and Canagarajah, N. (2007). Improving Fusion of Surveillance Images in Sensor Networks Using Independent Component Analysis. *IEEE Transactions on Consumer Electronics,* 53(3):1029–1035.

[11] Du, Y., He, X., and Calhoun, V. D. (2021). Smart (splitting-merging assisted reliable) inde pendent component analysis for brain functional networks. In *2021 43rd Annual International Conference of the IEEE Engineering in Medicine Biology Society (EMBC),* pages 3263–3266.

[12] Einevoll, G. T., Kayser, C., Logothetis, N. K., and Panzeri, S. (2013). Modelling and analysis of local field potentials for studying the function of cortical circuits. *Nature Reviews Neurscience,* 14(11):770–785.

[13] Esposito, F. and Goebel, R. (2011). Extracting functional networks with spatial independent component analysis. *Current Opinion in Neurology,* 24(4):378–385.

[14] Frost, W. N., Brandon, C. J., Bruno, A. M., Humphries, M. D., Moore-Kochlacs, C., Sejnowski, T. J., Wang, J., and Hill, E. S. (2015). Monitoring Spiking Activity of Many Individual Neurons in Invertebrate Ganglia. *Advances in Experimental Medicine and Biology,* 859:127–145.

[15] Głąbska, H., Potworowski, J., Łęski, S., and Wójcik, D. K. (2014). Independent Components of Neural Activity Carry Information on Individual Populations. *PLoS ONE,* 9(8):e105071.

[16] Gramfort, A., Luessi, M., Larson, E., Engemann, D. A., Strohmeier, D., Brodbeck, C., Goj, R., Jas, M., Brooks, T., Parkkonen, L., and Hämäläinen, M.S. (2013). MEG and EEG data analysis with MNE-Python. *Frontiers in Neuroscience,* 7(267):1–13.

[17] Gratiy, S. L., Devor, A., Einevoll, G. T., and Dale, A. M. (2011). On the estimation of population-specific synaptic currents from laminar multielectrode recordings. *Frontiers in neuroinformatics,* 5:32.

[18] Harris, C. R., Millman, K. J., Walt, S. J. v. d., Gommers, R., Virtanen, P., Cournapeau, D., Wieser, E., Taylor, J., Berg, S., Smith, N. J., Kern, R., Picus, M., Hoyer, S., Kerkwijk, M. H. v., Brett, M., Haldane, A., Río, J. F. d., Wiebe, M., Peterson, P., Gérard-Marchant, P., Sheppard, K., Reddy, T., Weckesser, W., Abbasi, H., Gohlke, C., and Oliphant, T. E. (2020). Array programming with NumPy. *Nature,* 585(7825):357–362.

[19] Harris Bozer, A. L., Uhelski, M. L., and Li, A.-L. (2017). Extrapolating meaning from local field potential recordings. *Journal of Integrative Neuroscience,* 16(1):107–126.

[20] Herreras, O., Makarova, J., and Makarov, V. A. (2015). New uses of LFPs: Pathway-specific threads obtained through spatial discrimination. *Neuroscience,* 310:486–503.

[21] Hill, E. S., Moore-Kochlacs, C., Vasireddi, S. K., Sejnowski, T. J., and Frost, W. N. (2010). Validation of Independent Component Analysis for Rapid Spike Sorting of Optical Recording Data. *Journal of Neurophysiology,* 104(6):3721–3731.

[22] Hong, G. and Lieber, C. M. (2019). Novel electrode technologies for neural recordings. *Nature Reviews Neuroscience,* 20(6):330–345.

[23] Hu, G., Waters, A. B., Aslan, S., Frederick, B., Cong, F., and Nickerson, L. D. (2020). Snowball ICA: A Model Order Free Independent Component Analysis Strategy for Functional Magnetic Resonance Imaging Data. *Frontiers in Neuroscience,* 14:569657.

[24] Hyvärinen, A. and Oja, E. (2000). Independent component analysis: algorithms and applications. *Neural Networks,* 13(4-5):411–430.

[25] Jung, T.-P., Makeig, S., McKeown, M. J., Bell, A. J., Lee, T.-W., and Sejnowski, T. J. (2001). Imaging brain dynamics using independent component analysis. *Proceedings of the IEEE,* 89(7):1107–1122.

[26] Kajikawa, Y. and Schroeder, C. E. (2011). How local is the local field potential? *Neuron,* 72(5):847–858.

[27] Makarov, V. A., Makarova, J., and Herreras, O. (2010). Disentanglement of local field potential sources by independent component analysis. *Journal of Computational Neuroscience,* 29(3):445 301–457.

[28] Makarova, J., Ibarz, J. M., Makarov, V. A., Benito, N., and Herreras, O. (2011). Parallel Readout of Pathway-Specific Inputs to Laminated Brain Structures. *Frontiers in Systems Neuroscience,* 5:77.

[29] Martínez-Cañada, P., Noei, S., and Panzeri, S. (2021). Methods for inferring neural circuit interactions and neuromodulation from local field potential and electroencephalogram measures. *Brain Informatics,* 8(1):27.

[30] Martínez-Cancino, R., Delorme, A., Truong, D., Artoni, F., Kreutz-Delgado, K., Sivagnanam, S., Yoshimoto, K., Majumdar, A., and Makeig, S. (2021). The open EEGLAB portal Interface: High-Performance computing with EEGLAB. *NeuroImage,* 224:116778.

[31] McConn, J. L., Lamoureux, C. R., Poudel, S., Palsson, B. O., and Sastry, A. V. (2021). Optimal dimensionality selection for independent component analysis of transcriptomic data. *BMC Bioinformatics,* 22(1):584.

[32] Meinecke, F., Ziehe, A., Kawanabe, M., and Müller, K.-R. (2002). A resampling approach to estimate the stability of one-dimensional or multidimensional independent components. *IEEE transactions on bio-medical engineering,* 49(12Pt2):1514–1525.

[33] Monakhova, Y. B. and Rutledge, D. N. (2019). Independent components analysis (ICA) at the "cocktail-party" in analytical chemistry. *Talanta,* 208:120451.

[34] Munro, E. and Kopell, N. (2012). Subthreshold somatic voltage in neocortical pyramidal cells can control whether spikes propagate from the axonal plexus to axon terminals: a model study. *Journal of Neurophysiology,* 107(10):2833–2852.

[35] Munro Krull, E., Sakata, S., and Toyoizumi, T. (2019). Theta Oscillations Alternate With High Amplitude Neocortical Population Within Synchronized States. *Frontiers in neuroscience,* 13:316.

[36] Naik, G. R. and Kumar, D. K. (2011). An Overview of Independent Component Analysis and Its Applications. *Informatica,* 35(1):63–81.

[37] Pedregosa, F., Varoquaux, G., Gramfort, A., Michel, V., Thirion, B., Grisel, O., Blondel, M., Müller, A., Nothman, J., Louppe, G., Prettenhofer, P., Weiss, R., Dubourg, V., Vanderplas, J., Passos, A., Cournapeau, D., Brucher, M., Perrot, M., and Duchesnay, E. (2011). Scikit-learn: Machine Learning in Python. *Journal of Machine Learning Research,* 12:2825–2830.

[38] Pesaran, B., Vinck, M., Einevoll, G. T., Sirota, A., Fries, P. ,Siegel, M., Truccolo, W., Schroeder, C. E., and Srinivasan, R. (2018). Investigating large-scale brain dynamics using field potential recordings: analysis and interpretation. *Nature Neuroscience,* 21(7):903–919.

[39] Reidl, J., Starke, J., Omer, D. B., Grinvald, A., and Spors, H. (2007). Independent component analysis of high-resolution imaging data identifies distinct functional domains. *NeuroImage,* 34(1):94–108.

[40] Sakurai, Y., Osako, Y., Tanisumi, Y., Ishihara, E., Hirokawa, J., and Manabe, H. (2018). Multiple Approaches to the Investigation of Cell Assembly in Memory Research—Present and Future. *Frontiers in Systems Neuroscience,* 12:21.

[41] Sinha, M. and Narayanan, R. (2022). Active Dendrites and Local Field Potentials: Biophysical Mechanisms and Computational Explorations. *Neuroscience,* 489:111–142.

[42] Smitha, K., Raja, K. A., Arun, K., Rajesh, P., Thomas, B., Kapilamoorthy, T., and Kesavadas, C. (2017). Resting state fMRI: A review on methods in resting state connectivity analysis and resting state networks. *The Neuroradiology Journal,* 30(4):305–317.

[43] Sompairac, N., Nazarov, P. V., Czerwinska, U., Cantini, L., Biton, A., Molkenov, A., Zhumadilov, Z., Barillot, E., Radvanyi, F., Gorban, A., Kairov, U., and Zinovyev, A. (2019). Independent Component Analysis for Unraveling the Complexity of Cancer Omics Datasets. *International Journal of Molecular Sciences,* 20(18):4414.

[44] Talebi, S. (2021). Independent Component Analysis (ICA): Finding hidden factors in data. *Towards Data Science,* `https://towardsdatascience.com/independent-component-analysis-ica-a3eba0ccec35`. Accessed 27 October 2023.

[45] Teeters, J. L., Harris, K. D., Millman, K. J., Olshausen, B. A., and Sommer, F. T. (2008). Data Sharing for Computational Neuroscience. *Neuroinformatics,* 6(1):47–55.

[46] Torres, D., Makarova, J., Ortuño, T., Benito, N., Makarov, V. A., and Herreras, O. (2019). Local and Volume-Conducted Contributions to Cortical Field Potentials. *Cerebral Cortex*, 29(12):5234–5254.

[47] Unakafova, V. A. and Gail, A. (2019). Comparing Open-Source Tool boxes for Processing and Analysis of Spike and Local Field Potentials Data. *Frontiers in Neuroinformatics,* 13:57.

[48] Yakushev, I., Drzezga, A., and Habeck, C. (2017). Metabolic connectivity: methods and application. *Current Opinion in Neurology,* 30(6):677–685.

[49] Zhang, N. and Nie, J. (2015). Independent Component Analysis Based Blind Source Separation Algorithm and its Application in the Gravity and Magnetic Signal Processing. 2015 *12th International Conference on Fuzzy Systems and Knowledge Discovery (FSKD)*, pages 269–273.

[50] Zhang, Q., Hu, G., Tian, L., Ristaniemi, T., Wang, H., Chen, H., Wu, J., and Cong, F. (2018). Examining stability of independent component analysis based on coefficient and component matrices for voxel-based morphometry of structural magnetic resonance imaging. *Cognitive Neurodynamics,* 12(5):461–470.

[51] Zhao, W., Li, H., Hu, G., Hao, Y., Zhang, Q., Wu, J., Frederick, B. B., and Cong, F. 367 (2021). Consistency of independent component analysis for FMRI. *Journal of Neuroscience Methods,* 351:109013.